Characteristics of High-Rate Energy Spectroscopy Systems Using HPGe Coaxial Detectors and Time-Variant Filters

C.L. Britton, T.H. Becker, T.J. Paulus, R.C. Trammell

EG&G ORTEC
100 Midland Road
Oak Ridge, TN 37830

Abstract

A high-rate, high-resolution gamma spectrometer system is described. The system consists of a reverse electrode HPGe coaxial detector, a transistor reset preamplifier, an active, semi-Gaussian prefilter, a gated integrator, and a unique data acquisition system consisting of a 10 µs, 13 bit ADC, fast FIFO memory, 8k by 23 bit data memory, and computer interface circuitry under the control of a Z-80A µP. The effects of the various components on the throughput are described and throughput data is presented. The resolution and peak shift for various shaping times are presented for count rates up to 1 Mcps input rate using a mixed ^{22}Na and ^{60}Co source. The low rate resolutions of ^{57}Co and ^{60}Co for various shaping times using either the semi-Gaussian or gated integrator output are discussed as well as the low energy resolution and peak shifts in the presence of high energy events.

Introduction

The need for gamma spectroscopy systems that will handle high input counting rates and give useful resolutions is increasing due to applications such as neutron activation analysis and post-accident monitoring in power plants. A system which will handle high input rates and give corresponding high throughput rates is presented in this paper. This work is an extension of previous work by the authors that dealt with time-invariant filters.[1] The system described here uses a time-variant filter to achieve useful output count rates for input count rates approaching 1 Mcps.

A block diagram of a high-rate spectroscopy system is shown in Figure 1. The principal components of this system are a HPGe detector, a transistor reset preamplifier (TRP), a time-variant shaping amplifier, a Multichannel Buffer (MCB) and a computer system. An optional counter/timer can be used to monitor the input count rate. The block diagram also shows the proper interconnection of the system for pileup rejection.

Various waveforms are also shown in Figure 1 and will be described in the next section.

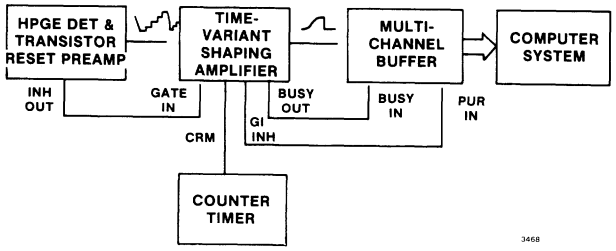

Figure 1. A Block Diagram of the High-Rate Gamma Spectroscopy System.

System Components

Detector-Transistor Reset Preamplifier

The detector used can be either the reverse electrode or the conventional HPGe coaxial configuration. The detector is coupled to a TRP similar to that reported by Landis, et al.[2] The basic configuration of the preamplifier is the same for both types of detectors. Only minor circuit changes are necessary to account for the difference in charge flow in detectors of different polarity.

A functional diagram of the TRP is shown in Figure 2. A charge loop is formed by the input FET Q1, the GAIN stage and the feedback capacitor C_{fb}. Charge is accumulated on C_{fb} due to detected nuclear events and detector leakage current. In a conventional charge loop, a high-value feedback resistor would be connected in parallel to C_{fb} to discharge this capacitor on a continuous basis. In the TRP, this resistor is replaced by Q2, D1, R, C2, current sources I_1 and I_2 and switch S. With S in the Normal position, the TRP operates as a charge sensitive preamplifier. When the output voltage reaches a preset dc value, switch S changes to Reset and current I_2 flows into C2 and Q2. This action causes Q2 to conduct and forms a new feedback loop. The forward gain path now consists of Q2, Q1, and GAIN. The new feedback path consists of R and C2. The new circuit configuration acts as an integrator for current I_2 forcing the output voltage negative and discharging C_{fb}. The switch S returns to the Normal position when C_{fb} is completely discharged.

The TRP has several important advantages compared to the conventional resistive fedback scheme normally found in high-resolution HPGe spectroscopy systems. First, the absence of the feedback resistor eliminates the need for pole-zero compensation, a critical adjustment in the optimization of a standard spectroscopy system operating at high input count rates. Second, a high value feedback resistor is a frequency dependent impedance that can cause varying amounts of undershoot

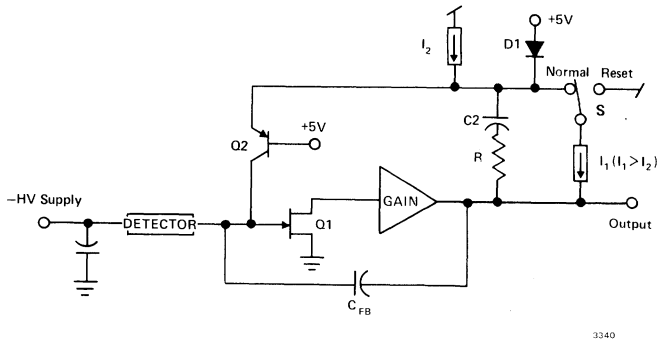

Figure 2. A Block Diagram of the Transistor Reset Preamplifier (TRP).

0018-9499/84/0002-0455$01.00 © 1984 IEEE

or overshoot on the trailing edge of the output pulse of the main amplifier.[3] A system that can be properly pole-zero adjusted at 6 μs can have severe undershoot at 0.25 μs. Third, since the TRP only operates over a limited dynamic range, it can have excellent linearity resulting in improved resolution and reduced peak shift at very high input count rates. The TRP has an energy rate capability of greater than 800 GeV/sec., and is fabricated in a streamlined configuration.[4]

Some important waveforms associated with a TRP system are shown in Figure 3. Most characteristic of a TRP system is the ramp waveform shown in Figure 3a. As described above, the TRP integrates charge from nuclear events causing the output voltage to rise. When the output reaches a preset voltage, indicated by the dashed line, the reset sequence begins. First there is a waiting period T2, nominally 17 μs, to allow time to process the last pulse that could cause the reset level to be reached. This precludes the loss of large amplitude pulses that would have the greatest probability of causing reset. The actual reset interval occurs during time T3, nominally 5 μs. The rapid return to the baseline of the TRP output can cause a negative overload pulse at the output of the shaping amplifier. This effect is shown in Figure 3b. The overload period during which the amplifier is disabled is labeled T_{AOL}. A blocking signal is provided by the TRP to the shaping amplifier to block signal processing during this overload period. Figure 3c shows this pulse, T_{INH}, which begins at the start of T3 and is extended beyond the reset time by a one-shot whose length depends on the amplifier shaping time constant. Based on the waveform shown in Figure 3a, the fractional deadtime of the TRP is given by the ratio T3/T1. Alternately, the %DT is also given by

$$\%DT^{TRP} = \frac{T3}{\frac{V_{RAMP}}{(ER)(CG)} + T_2 + T_3} \times 100\% \qquad (1)$$

where ER is the energy rate product of the signal at the TRP input, and CG is the conversion gain of the TRP, nominally 200 mV/MeV. In most cases, the TRP does not contribute directly to the overall system deadtime due to the masking effect of the amplifier overload following TRP reset. This case will be considered in the next section.

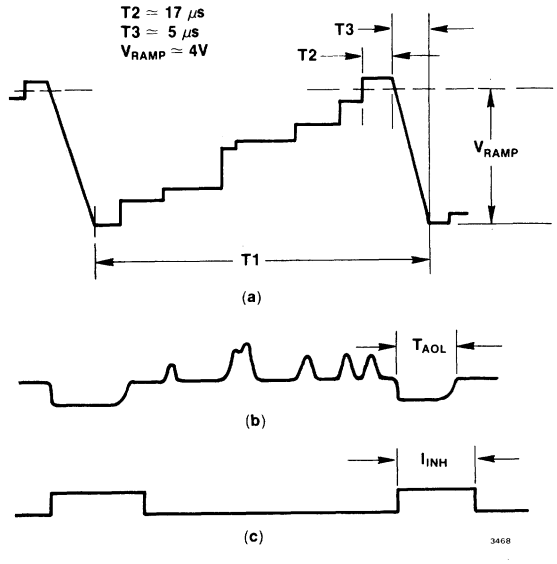

Figure 3. Important Waveforms in a TRP System.

Shaping Amplifier

A simplified block diagram of the time-variant shaping amplifier is shown in Figure 4. The shaping amplifier consists of a unipolar semi-Gaussian pulse amplifier acting as a prefilter for a gated integrator.[5-10] The prefilter output, UNI, is inverted by amplifier A1 before being processed by the inverting gated integrator section to produce output GI. While a signal is being processed, switch S1 is closed; S2 and S3 are open. At the end of the pulse processing time, S1 is opened while S2 and S3 are closed. Any charge stored on the integrating capacitor will be discharged at this time, forcing the GI output to zero. The total processing time is approximately eight to ten times the shaping time constant, τ. Typical UNI and GI pulse shapes are shown in Figure 5. The time-variant shaping amplifier is fabricated as a 2-wide NIM module.[11]

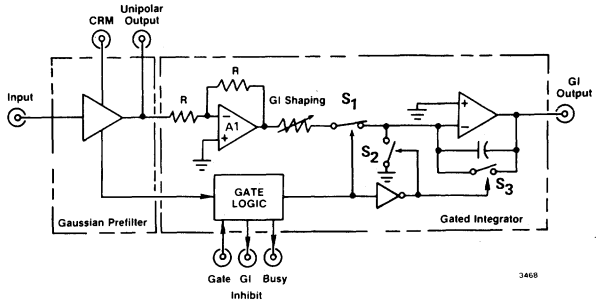

Figure 4. A Simplified Block Diagram of the Time-Variant Shaping Amplifier.

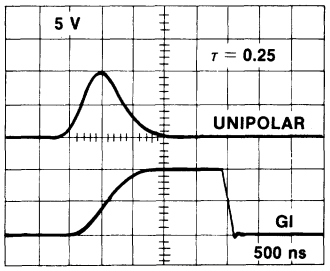

Figure 5. Unipolar and Gated Integrator Output Waveforms.

A time-variant filter, such as a gated integrator, is an essential element in a high-throughput system using HPGe detectors. In order to process a large number of nuclear events in a short period of time, each pulse duration must be short in order to reduce pileup. However, a pulse duration time that is too short compared to the finite charge collection time of the HPGe detector will result in spectral peak distortion due to ballistic deficit.[12] Figure 6 shows the distortion due to charge collection time effects when using a semi-Gaussian output at 0.5 μs shaping time constant. Figure 7 shows the results of an equivalent experiment using a shorter shaping time of 0.25 μs and GI shaping. Note the dramatic improvement in spectral peak shape.

Although short shaping times reduce pulse pileup, some pileup always remains in a pulse processing system with a random input signal. Of interest to the spectroscopist is the unpiled-up output rate. For semi-Gaussian filters, the unpiled-up output rate is given by[13]

$$r_o = r_i \exp(-T_D r_i) \qquad (2)$$

where r_o is the unpiled-up output count rate, r_i is the

input count rate, and T_D is the deadtime or effective processing time of the amplifier. The value of T_D is equal to the sum of the effective amplifier pulse width, T_W, and the time-to-peak of the amplifier output pulse, T_P. This type of deadtime in the shaping amplifier is referred to as an extending deadtime since a second event arriving before the end of the initial deadtime extends the deadtime by an additional amplifier pulse width, T_W, from the occurrence of the second pulse. When using a pileup inspector circuit, the value of T_D is given either by the sum of T_W and T_P or by the sum of T_P and the pileup inspection time, whichever is larger. The maximum mean output rate occurs when the mean input rate equals $1/T_D$.

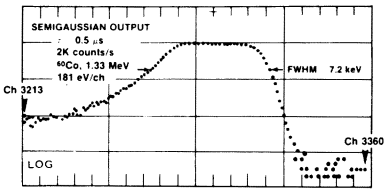

Figure 6. Distortion Due to Charge Collection Time Effects When Using Semi-Gaussian Output at Short Shaping Time Constants.

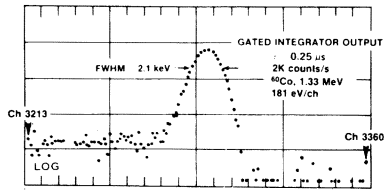

Figure 7. Elimination of Charge Collection Time Effects With the Gated Integrator.

Spectroscopy systems also have a deadtime which is caused by the digitizing time of the Analog-to-Digital Converter (ADC). This deadtime is a non-extending deadtime since events arriving during the digitizing time are ignored. For non-extending deadtime the output rate is given by[13]

$$r_o = \frac{r_i}{1 + r_i T_M} \qquad (3)$$

where T_M is the digitizing time for the ADC and memory. The maximum obtainable output count rate is $1/T_M$ and occurs at r_i equal to infinity.

When the ADC is considered as part of the spectroscopy system the deadtimes of the amplifier and the ADC are in series. The combination of the extending deadtime of the amplifier followed by the non-extending deadtime of the ADC is given by[13]

$$r_o = \frac{r_i}{\exp\left(r_i(T_W+T_P)\right)+r_i\left(T_M-(T_W-T_P)\right)\,U\left(T_M-(T_W-T_P)\right)} \qquad (4)$$

where $U(T_M - (T_W - T_P))$ is a unit step function which changes value from 0 to 1 when T_M is greater than $(T_W - T_P)$. Equation (4) reduces to Equation (2) when T_M is less than $(T_W - T_P)$.

The combined effects of amplifier and ADC deadtime on the system throughput are shown in Figures 8 and 9. The effective deadtime for the gated integrator with an integration time, T_I, is $2T_I$ since $T_P = T_W = T_I$ and $T_D = T_P + T_W$. The gated integrator throughput curves use a value of 2.5 μsec. for T_I. Figure 8 shows the system throughput performance for 2 μs semi-Gaussian shaping. The upper curve is the limit imposed by the amplifier. As expected, a 10 μs conversion ADC provided greater throughput than a Wilkinson converter with an average conversion time of 40 μs.

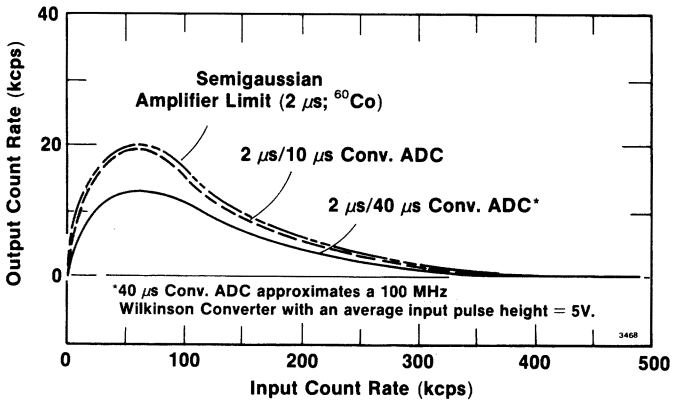

Figure 8. Semi-Gaussian (Unipolar) Throughput With ADC.

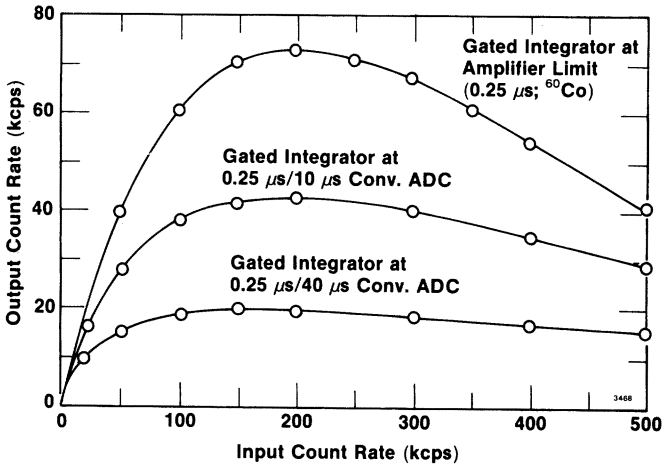

Figure 9. Gated Integrator Throughput With ADC.

A dramatic improvement in system throughput can be achieved using 0.25 μs GI pulse shaping as shown in Figure 9. Experimental data presented later in this paper will demonstrate that there is little loss in resolution when using 0.25 μs GI especially at high input count rates. Note that the maximum throughput for the 0.25 μs GI is over 70,000 cps compared to 20,000 cps for the 2 μs semi-Gaussian case. Also, there are corresponding higher throughputs for the 10 μs and the 40 μs conversion time ADC's when used with the GI shaping. Of equal importance is the presence of significant throughput with the GI system even at ultra high input rates, greater than 400,000 cps.

The TRP can cause a deadtime in the amplifier due to amplifier overload resulting from the TRP reset signal. The resulting deadtime in the amplifier can be estimated by replacing T3 in Equation (1) with the

amplifier overload time T_{INH} yielding

$$\%DT^{AOL} = \frac{T_{INH}}{\frac{V_{RAMP}}{(ER)(CG)} + T2 + T3} \times 100\ \% \qquad (5)$$

Note in Equation (5) that the deadtime can approach 100% as the time between reset pulses in the TRP approaches T_{INH}. Equation (5) modifies the throughput data described earlier to obtain the overall system throughput.

Multichannel Buffer

A functional diagram of the Multichannel Buffer, MCB, is shown in Figure 10. The MCB consists of a 10 µs, 13 bit successive approximation ADC followed by a 40-word fast FIFO memory for derandomization. The MCB is under the control of a Z-80A microprocessor. Data memory is 8000 channels by 24 bits. The MCB I/O capabilities include 20-mA current loop, RS-232 serial interface, optional IEEE-488 parallel interface, and optional dual-ported memory for direct data transfer. Deadtime correction is selectable between extended livetime correction or realtime counting loss correction. Presets can be independently set for different memory segments on realtime, livetime, ROI peak, ROI integral or data overflow. The program memory is 8-bit words with 24k ROM and 6k RAM. The differential linearity of the ADC is less than 1% and integral linearity is less than 0.05% over 99% dynamic range. The maximum average throughput for the MCB is 40,000 cps. The MCB is fabricated in a 2-wide NIM module.[14]

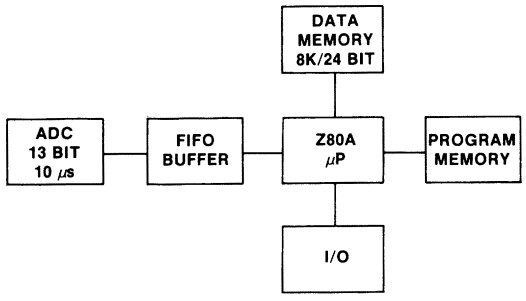

Figure 10. A Simplified Block Diagram of the Multichannel Buffer (MCB).

When combined with any one of a variety of computers, the MCB performs the traditional function of a very high speed multichannel analyzer. Commands are issued to the MCB using the recently approved Standard NIM Digital Bus (NIM/GPIB).[15] The MCB is especially suited for use with the new generation of personal computers such as the DEC PROFESSIONAL* series or the IBM PC**. The MCB is equally easy to interface to larger machines such as the DEC VAX* PDP-11* series computers.

The MCB can select by computer control one of two methods of deadtime correction. The more traditional method of deadtime correction extends the realtime to achieve a specified or set value of livetime. Using this technique, each event converted by the ADC in the MCB adds one to memory in the channel corresponding to the energy of the event digitized. When realtime counting loss deadtime correction is selected, a number greater than one can be added to memory in the appropriate channel depending on the deadtime of the system at the instant the input event is digitized. For a 10% deadtime, a value of 1 is added to memory 90% of the time and a value of 2 is added 10% of the time. With a 50% deadtime, an average value of 2 is added to memory for each input digitized. With a 90% deadtime, an average value of 10 is added to memory for each input conversion. The major application of realtime counting loss deadtime correction is for high input rate experiments having lines with rapidly changing activity. In this method of deadtime correction the integral number of counts in a peak can be substantially greater than the number of events digitized that would fall into that peak. Consequently, normal $\sqrt{N}$ statistical analysis does not apply.

System Performance

The high-rate spectroscopy system described above was subjected to several performance tests. The system was connected as shown in Figure 1. The TRP INH OUT signal was connected to the GI GATE IN to block the GI during the TRP reset and for any subsequent amplifier overload period. The GI INH signal connects to the MCB pileup rejection input, PUR IN, to prevent an ADC conversion when a piled-up signal is present. The GI BUSY OUT signal connects to the MCB BUSY IN to account for the entire system livetime/deadtime. An optional counter/timer can be connected to the CRM output to monitor the input count rate. Care must be taken when reading the CRM rate to correctly account for deadtime losses in the CRM circuitry for input count rates exceeding several hundred kcps. Deadtime measurements of the CRM circuitry indicated a 1% error at 100 kcps, a 12% error at 460 kcps, and a 25% error at 1000 kcps. Thus a CRM reading of 750 kcps corresponds to an actual input rate of over 1,000,000 cps.

The system resolution at 1.33 MeV ^{60}Co as a function of input count rate is shown in Figure 11. Data was taken using a combination of ^{22}Na and ^{60}Co sources. Using 2 µs semi-Gaussian shaping yielded resolution of 1.86 keV at low rate and under 2 keV for count rates up to about 120 kcps. Using 0.5 µs GI shaping yielded a low rate resolution of 2.15 keV and remained less than 3.0 keV for input rates up to 400 kcps. Using 0.25 µs GI shaping yielded a low rate resolution of 2.22 keV which remained less than 3.0 keV for input rates up to 700 kcps and less than 4.0 keV for input rates in excess of 1000 kcps.

Peak shift for 2 µs semi-Gaussian shaping was approximately 0.1 keV for input count rates up to 100 kcps. Peak shift was approximately 0.5 keV for

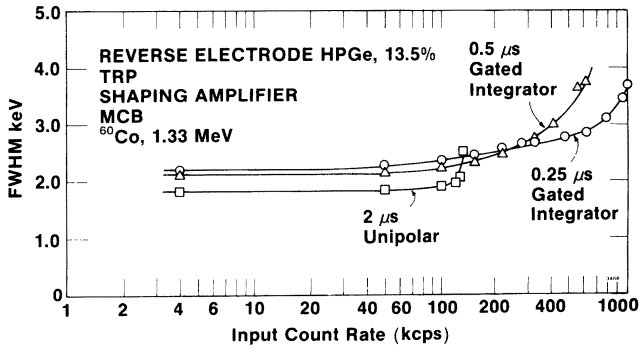

Figure 11. Resolution as a Function of Input Count Rate.

*DEC PROFESSIONAL, DEC VAX, and PDP-11 are registered trademarks of Digital Equipment Corporation.
**IBM PC is a registered trademark of International Business Machines.

0.5 μs GI for input count rates up to 200 kcps and approximately 2 keV for up to 400 kcps. Peak shift for 0.25 μs GI was approximately 1 keV for input count rates up to 100 kcps, less than 2.5 keV for up to 500 kcps, and less than 2.7 keV for up to 1000 kcps.

The quality of the spectra data available at these ultra-high input count rates is shown in Figure 12. This data was taken using 0.25 μs shaping. Figure 12a shows data at an input rate of 5 kcps. The lines of ^{22}Na and ^{60}Co are clearly evident. Figure 12b shows spectral data for 105 kcps input count rate, Figure 12c for 460 kcps input count rate, and Figure 12d for 1050 kcps input count rate. Some high-side tailing is evident for input count rates approaching 1 Mcps.

A graph of the complete system throughput as a function of input count rate is shown in Figure 13. The maximum output rate was approximately 30 kcps and occurred at approximately 125 kcps input count rate. The peak output rate occurred at a lower than anticipated input count rate due to the effects of amplifier overload caused by the TRP reset signal. The value of T_{INH} was nominally 40 μs for this experiment. Throughput can be increased at the expense of resolution by reducing T_{INH}.

Low rate resolution data is shown in Figure 14, and illustrates charge collection effects as a function of shaping time constant. Resolution of the ^{60}Co 1.33 MeV line begins to deteriorate for time constants less than 1 μs when using semi-Gaussian pulse shaping.

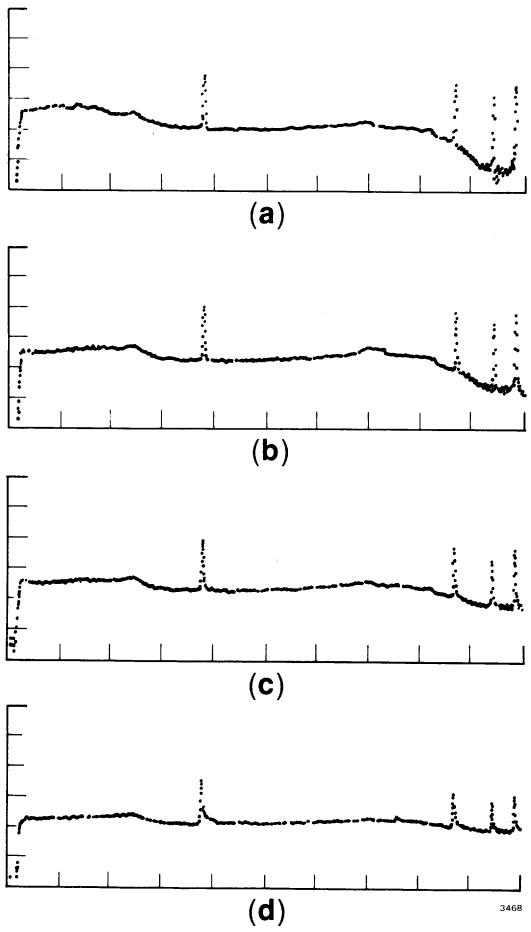

Figure 12. Spectra Obtained With the High-Rate Spectroscopy System Using ^{22}Na and ^{60}Co: (a) 5 kcps, (b) 100 kcps, (c) 500 kcps and (d) 1 Mcps.

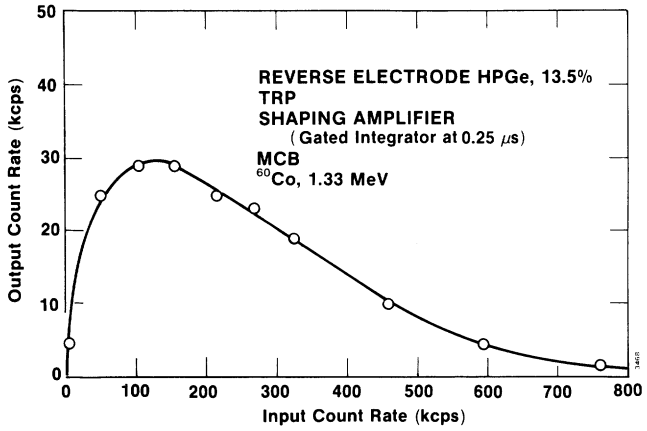

Figure 13. System Throughput for the Total High-Rate Spectroscopy System.

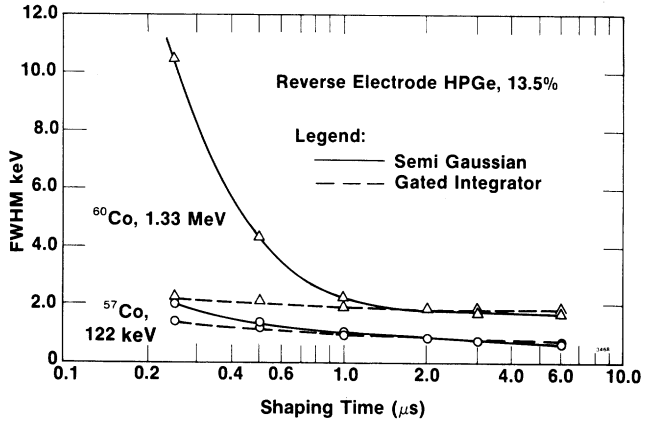

Figure 14. Resolution as a Function of Shaping Time Constant for Semi-Gaussian and Gated Integrator Pulse Shaping.

At 0.25 μs time constant, GI shaping is a factor of approximately 4.8 times better in resolution than semi-Gaussian shaping for this high energy. The difference in shaping technique is much less evident at lower energies. Figure 14 also shows data for the ^{57}Co (122 KeV) line. Low energy resolution is more dependent on noise than on charge collection effects, and hence, there is less divergence between the two pulse shaping techniques. However, charge collection can still contribute to line broadening at short shaping times.

The effect of overloading pulses on the resolution of non-overloading pulses is shown in Figure 15. In this experiment, the overloading source is ^{60}Co (1.33 MeV) and the non-overloading source is ^{57}Co (122 keV).

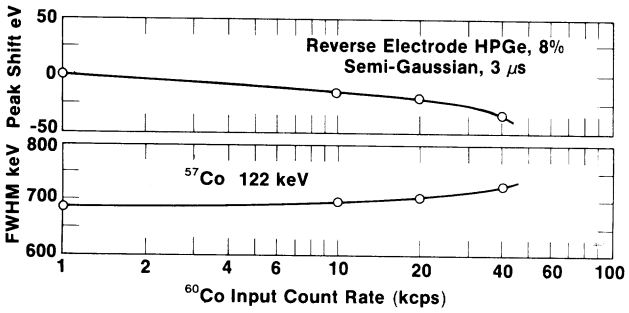

Figure 15. Effect of ^{60}Co Count Rate on ^{57}Co (122 keV) Resolution and Peak Shift.

Conclusions

A high-rate, high-resolution gamma spectrometer using a time-variant filter was described. The effects of the various components on the throughput were described. Measured resolution data for both time-invariant and time-variant filters was presented. Data was reported for count rates up to 1 Mcps. Spectral data confirmed that useful output can be achieved even at this ultra-high input count rate.

Acknowledgments

The high rate spectroscopy system described here is the result of the efforts of many. In particular, the authors acknowledge the direct contributions of D. Cole, J. Ursery, and the firmware development team in the digital circuitry development of the MCB. T. Mayhugh and M. Casey also made direct contributions in the early development of the fast ADC and state control machine. Thick film hybrid circuitry was developed by P. Hubbard and her fine staff; and detectors were supplied by G. Martin and his production staff. The authors also are grateful to L. Sams for typing the manuscript and to J. Schall for preparing the photocopy.

References

1. T.H. Becker, E.E. Gross, and R.C. Trammell, "Characteristics of High-Rate Energy Spectroscopy Systems with Time-Invariant Filters," IEEE Trans. Nucl. Sci., NS-28, No. 1, pp. 598-602, (1981).

2. D.A. Landis, C.P. Cork, N.W. Madden, and F.S. Goulding, "Transistor Reset Preamplifier for High-Rate, High-Resolution Spectroscopy," IEEE Trans. Nucl. Sci., NS-29, No. 1, pp. 619-624, (1982).

3. P.W. Nicholson, Nuclear Electronics, J. Wiley and Sons, New York, (1974), pp. 183-184.

4. "Solid State Photon Detector Operator's Manual, Gamma-X Plus Series," EG&G ORTEC, Oak Ridge, TN, 1983.

5. V. Radeka, "Trapezoidal Filtering of Signals from Large Germanium Detectors at High Rates," NIM 99, (1972), pp. 525-539.

6. N. Karlovac and T.V. Blalock, "Resolution and Count Rate Characteristics of the Gated Integrator Nuclear Amplifier," IEEE Trans. Nucl. Sci., NS-22, No. 1, pp. 452-456, (1975).

7. G.P. Westphal, "On the Performance of a High-Rate Gamma Spectroscopy System," NIM 138, (1976), pp. 467-470.

8. K. Kandiah and G. White, "Status at Harwell of Opto-Electronic and Time-Variant Signal Processing for High Performance Nuclear Spectrometry with Semiconductor Detectors," IEEE Trans. on Nucl. Sci., NS-28, No. 1, pp. 613-620, (1981).

9. J.H. McQuaid, D.R. Brown, T. Gozani, and H. Bozorgmanesh, "High Rate Spectroscopy for On-Line Nuclear Coal Analyzer (Nucoalyzer)," IEEE Trans. Nucl. Sci., NS-28, No. 1, pp. 304-307, (1981).

10. F.S. Goulding and D.A. Landis, "Signal Processing for Semiconductor Detectors," IEEE Trans. on Nucl. Sci., NS-29, No. 3, pp. 1125-1141, (1982).

11. "Model 673 Spectroscopy Amplifier and Gated Integrator Operating and Service Manual," EG&G ORTEC, Oak Ridge, TN, 1983.

12. Nicholson, pp. 92-95, 148.

13. R. Jenkins, R.L. Gould, and D.A. Gedcke, Quantitative X-Ray Spectroscopy, Marcel and Dekker, Inc., New York, (1980).

14. "Operator's Manual for EG&G ORTEC's ADCAM Model 918 Multichannel Buffer Module," EG&G ORTEC, Oak Ridge, TN, 1983.

15. U.S. NIM Committee, "Standard NIM Digital Bus (NIM/GPIB)," U.S. Dept. of Energy, Wash. D.C., August, 1983.